Available online at www.sciencedirect.com

ScienceDirect

International Journal of Solids and Structures 44 (2007) 659–671

INTERNATIONAL JOURNAL OF SOLIDS and STRUCTURES

www.elsevier.com/locate/ijsolstr

Analysis of the strain field in the vicinity of a crack-tip in an in-plane isotropic paper material

P. Isaksson [a,*], R. Hägglund [b]

[a] *Department of Engineering Physics, Mid Sweden University, SE-851 70 Sundsvall, Sweden*
[b] *SCA Packaging Research, Box 716, SE-851 21 Sundsvall, Sweden*

Received 19 January 2006; received in revised form 10 April 2006
Available online 11 May 2006

Abstract

Strains, computed by the finite element method, are evaluated and compared to an experimentally determined strain field. The analyzed low-density paper has been designed to ensure bond–breakage as the dominating damage mechanism and the paper material is approximately in-plane isotropic. An optical non-contact displacement measuring system has been used in fracture tests to determine the strain field in the crack-tip region of a pre-fabricated crack. Additionally, acoustic emission monitored tensile tests have been conducted to determine onset and evolution of damage processes and thereby enabling calibration of required constitutive parameters. The results suggest that the investigated paper material can tolerate significantly higher strains than what is predicted by a classic elastic–plastic J_2-flow theory. Immediately before onset of the final fracture (i.e., localization), the experimental measured normal strain in the near-tip region is around 60% higher than the computed strain when using exclusively an elastic–plastic theory for the corresponding load while the strain computed utilizing a non-local damage theory is of the same order of magnitude as the experimentally measured strain. Hence, it seems essential to include a non-local continuum theory to describe strains in the near-tip region quantitatively correct for paper materials. It is demonstrated that path independence of the well-known J-integral does not prevail for this class of material models. Only for the special situation of a homogenous damage field in the crack-tip region may the stress and strain fields be described by the well-known HRR-solutions.

Keywords: Non-local gradient damage theory; Bond failure; Tissue paper material; Strain; crack-tip region

1. Introduction

If a flaw is introduced in the web in any stage in the paper manufacturing process, it may cause catastrophic failure because of locally raised stresses. Consequently, fracture toughness is a crucial property for paper materials in order to obtain high productivity. Paper essentially consists of a planar stochastic network of discontinuous cellulose fibers. The fracture behavior of paper has been subject of research efforts for the past

* Corresponding author.
E-mail address: per.isaksson@miun.se (P. Isaksson).

0020-7683/$ - see front matter
doi:10.1016/j.ijsolstr.2006.05.007

three decades, cf. Niskanen (1993) for a review of the subject. While most previous work in this area deals with fracture of dense cellulose fiber networks such as packaging paper (cf. Westerlind et al., 1991) or graphic (cf. Swineheart and Broek, 1995), relatively little has been done to characterize fracture of open cellulose networks such as tissue paper (low-basis-weight paper). The failure behavior of this type of paper is often dominated by fiber-to-fiber bond breaks due a combination of weak bonds and a low degree of inter-fiber bonding. Fracture of this class of material was recently studied in an investigation by the authors (Hägglund and Isaksson, in press) where it was concluded that the classical theory of linear elastic fracture mechanics could not properly predict the failure load for an opening mode crack in a paper web below a crack length of ≈50 mm. This is assumed to be a result of that a wide damage zone is developing in the crack-tip region and locally causes a stiffness degradation and thereby alters the shape of the stress field ahead of the crack.

The effect of damage on the fracture behavior has been studied by several researchers (among others: Ortiz, 1987; Hutchinson, 1987; or Ravichandran and Liu, 1998). In several previous investigations by the authors (cf. Hägglund and Isaksson, in press; or Isaksson and Hägglund, 2005) it has been reported that the continuum damage mechanics (CDM) concept seems promising to describe the constitutive behavior of paper. A CDM approach is phenomenological with no attempt to explain the damage process itself and an internal variable that characterizes the accumulated amount of damage is introduced. The non-local micro-structural effect, caused by the manner in which neighboring constituents of the fiber network interact, is accounted for by invoking a gradient formulation (cf. Geers, 1997; or de Borst et al., 1999) in the constitutive model. The model has proved to properly describe a mode I (opening mode) fracture behavior for a wide range of initial crack lengths when a length parameter controlling the non-locality was set equal to around twice the fiber length, Hägglund and Isaksson (in press). However, the use of a non-local damage theory for fracture analysis of open cellulose structures needs further verification.

As a logical continuation of the previous work mentioned above, this study deals with the strain distribution in the vicinity of a macroscopic crack in a low-basis-weight paper under loading conditions of opening mode. Calculated strains, by the finite element method, are compared to an experimentally measured strain field. An optical non-contact displacement measuring system is used in fracture tests to determine the strain field in the crack-tip region of a pre-fabricated crack. A small domain in the vicinity of a crack-tip is monitored by a CCD camera system and a sequence of photographic images at various load levels is recorded during loading. Subsequently, consecutive images are compared using an image analysis system, which traces individual points and generates strain fields through spatial numerical differentiation of the displacement field. Additionally, acoustic emission monitored tensile tests of paper specimens are conducted to determine onset and evolution of damage processes and thereby enabling calibration of the required constitutive parameters.

2. Theory

The low-basis-weight paper material discussed in this investigation is assumed to exhibit approximately in-plane isotropic damage-elastic–plastic behavior and the governing micro fracture mechanism is understood to be fiber-to-fiber bond failure. The assumption of fiber-to-fiber bond failure will be discussed in Section 3. Plane stress conditions are assumed to prevail. Continuum damage mechanics is used to describe damage in the body, i.e., damage is treated in a "smeared out" sense on a continuum level. Damage degradation is governed by an isotropic internal variable denoted D, where virgin material is characterized by $D = 0$ while $D = 1$ corresponds to a fully ruptured. The assumption of one single isotropic damage variable is justified because of the nature of the prevailing damage mechanism, i.e., fiber-to-fiber bond breaks. If a bond is loaded in the plane of the sheet, it is believed that the strength of such bond is independent of in which direction it is loaded. Fiber breakage is a critical factor for paper strength only if the bonds are very strong or the fibers weak. It has been shown that in dense anisotropic paper structures, where fiber breaks is the dominating damage mechanism, one damage parameter for each in-plane direction is required to describe the damage behavior properly (cf. Isaksson et al., 2004). This may be explained by that the fiber breakage is a directional dependent failure mechanism because the fracture plane is perpendicular to the direction of the fiber.

An assumption of the postulate of complementary elastic energy equivalence is made (cf. Hansen and Schreyer, 1994) which means that the elastic energy density in a material element of a damaged material is

of the same form as that of an undamaged material except that the physical damaged stress tensor σ_{ij} is replaced by an effective stress tensor $\hat{\sigma}_{ij}$ according to

$$\sigma_{ij} = (1 - D)\hat{\sigma}_{ij}. \tag{1}$$

The effective stress $\hat{\sigma}_{ij}$ and its work conjugate, the effective strain $\hat{\varepsilon}_{ij}$, are referred to a fictitious surface in the material that transmits the internal forces. As a consequence of the adopted postulate of elastic energy equivalence, the non-linear relation $(1 - D)^2$ reflects the level of degradation of the isotropic elastic stiffness tensor C_{ijkl} for the virgin material. Hence, the physical damaged elastic stress–strain relation is given by $\sigma_{ij} = (1 - D)^2 C_{ijkl}\varepsilon^{e}_{kl}$.

If it is assumed that one scalar parameter D describes damage in a point, then the driving force for damage evolution in that point is given by the local damage energy release rate $Y = \partial\psi/\partial D$, where $\psi = \hat{\sigma}_{ij}C^{-1}_{ijkl}\hat{\sigma}_{kl}/2$ is the elastic stress energy density. According to the postulate of elastic energy equivalence, one obtains with use of (1) and assuming D is isotropic,

$$Y = (1 - D)^{-3}\sigma_{ij}C^{-1}_{ijkl}\sigma_{kl}. \tag{2}$$

However, to account for long ranging micro structural effects a non-local theory has to be included to properly describe microscopic fracture progression. This is physically motivated by the microstructure of the paper material as it is considered as an inhomogeneous solid containing many long fibres connected in a network. At any point those fibres apply non-local actions. There exist different techniques to incorporate non-locality. Examples of such formulations include non-local integral formulations (cf. Kröner, 1967; or Eringen and Edelen, 1972) and gradient theories (cf. Geers, 1997; or de Borst et al., 1999). A review of non-local models can be found in Jirásek (1998). Pijaudier-Cabot and Bazant (1987) originally proposed the non-local technique discussed here and the authors have fruitfully applied the concept to analyze tensile response of different types of paper materials (cf. Isaksson et al., 2006; or Isaksson and Hägglund, 2005).

For sufficiently smooth fields of Y a non-local counterpart to Y in a point p can be obtained from a Taylor expansion around p (cf. Pijaudier-Cabot and Bazant, 1987; Lasry and Belytschko, 1988; Mühlhaus and Aifantis, 1991; or Peerlings et al., 1996),

$$\overline{Y}(p) = Y(p) + c_2\nabla^2 Y(p) + c_4\nabla^4 Y(p) + \cdots, \tag{3}$$

where the Laplacian operator is $\nabla^2 = \sum_i \partial^2/\partial x_i^2$ and $c_{2m} = \frac{1}{m!}[l^2/2]^m$; $m = 1, 2\ldots$. The gradient sensitivity parameter l is a characteristic length that controls the range of non-local actions. In (3) it is assumed that the non-local counterpart to Y is spherically symmetric (Gaussian) distributed whereupon all odd terms vanish. Fig. 1 shows a schematic illustration of an isotropic Gaussian weight function around a point p and its relation to the characteristic length l.

Continuing to follow the direction pointed out by Peerlings et al. differentiate (3) two times and substitute back into (3), a truncated implicit gradient enhanced formulation is obtained that is suitable to incorporate in finite element analyses,

$$\overline{Y}(p) - \frac{1}{2}l^2\nabla^2\overline{Y}(p) = Y(p). \tag{4}$$

In (4) derivatives of order four and higher have been neglected and it is assumed that $\overline{Y}$ admit at least Fréchet derivative. Needless to say, in a homogenous stress field all stress gradients vanishes and $\overline{Y} \to Y$. When solving (4), a natural boundary condition of a vanishing gradient is used along the boundary surrounding the entire problem domain, i.e., $q\nabla\overline{Y} = 0$ where q is the outward normal to the boundary. The interested reader is

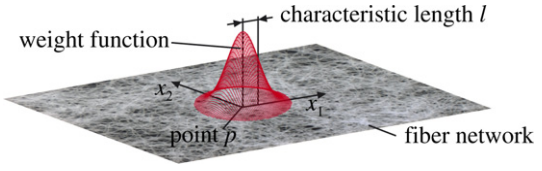

Fig. 1. Illustration of an isotropic Gaussian weight function around a point p in a region determined by the characteristic length l.

advised to Peerlings et al. (1996) or Geers (1997) for a throughout description of the derivation of the theory discussed here.

On incremental form, a damage evolution law is formulated as:

$$\mathrm{d}D = \begin{cases} k(1-D)\mathrm{d}\overline{Y} & \text{for } \overline{Y} = R \\ 0 & \text{else} \end{cases} \tag{5}$$

where k is a material parameter that can be determined in experiments. The threshold R represents an isotropic damage behavior and is the maximum value that $\overline{Y}$ has reached during the deformation history with the initial threshold value Y_0. It has been reported in earlier studies that the damage evolution law (5) describes material degradation of different types of paper reasonably well, cf. Hägglund and Isaksson (in press) or Isaksson et al. (2006).

As the low-basis-weight paper material considered is approximately isotropic damage-elastic–plastic, an assumption of an isotropic strain hardening plasticity behavior of the material is made. Assuming a J_2-flow theory of plasticity, the yield surface ϕ is given by:

$$\phi = \hat{\sigma}_{\mathrm{e}}^2 - H^2 \leqslant 0, \tag{6}$$

where $\hat{\sigma}_{\mathrm{e}} = \left(\frac{3}{2}\hat{s}_{ij}\hat{s}_{ij}\right)^{1/2}$ is the von Mises equivalent stress. The deviatoric effective stress tensor is given by $\hat{s}_{ij} = \hat{\sigma}_{ij} - \delta_{ij}\hat{\sigma}_{kk}/3$ where repeated index assumes summation and δ_{ij} is the Kronecker delta. It is observed that the plastic processes are connected to the effective stress since $\hat{\sigma}_{ij}$ is referred to a surface in the material that transmits the internal forces. The plastic threshold H is the maximum value $\hat{\sigma}_{\mathrm{e}}$ has reached during the deformation history with the initial value σ_0.

Assuming small deformations, the total physical strain increment $\mathrm{d}\varepsilon_{ij}$ is given by the sum of an elastic part and a plastic part, $\mathrm{d}\varepsilon_{ij} = \mathrm{d}\varepsilon_{ij}^{\mathrm{e}} + \mathrm{d}\varepsilon_{ij}^{\mathrm{p}}$. Normality of the plastic strain increment requires that:

$$\mathrm{d}\varepsilon_{ij}^{\mathrm{p}} = \lambda \partial\phi/\partial\hat{\sigma}_{ij}, \tag{7}$$

where the outward normal of the yield surface is given by $\partial\phi/\partial\hat{\sigma}_{ij} = 3\hat{s}_{ij}$ and λ is a plastic multiplier that can be determined in a tensile test. As a result of energy conservation, the relation $\hat{\varepsilon}_{ij}^{\mathrm{e}} = (1-D)\varepsilon_{ij}^{\mathrm{e}}$ of the elastic strains holds. For the plasticity process, Chow and Lu (1992) showed that the plastic work rate is conserved during a load increment, i.e. the relation between the plastic strain increments is:

$$\mathrm{d}\hat{\varepsilon}_{ij}^{\mathrm{p}} = (1-D)\mathrm{d}\varepsilon_{ij}^{\mathrm{p}}. \tag{8}$$

Assuming that the elastic-damage stiffness remains constant within each stress/strain increment (cf. AbuAl-Rub and Voyiadjis, 2003) and by using the elastic stress–strain relationship $\mathrm{d}\hat{\sigma}_{ij} = C_{ijkl}\mathrm{d}\hat{\varepsilon}_{kl}^{\mathrm{e}} = C_{ijkl}(\mathrm{d}\hat{\varepsilon}_{kl} - \mathrm{d}\hat{\varepsilon}_{kl}^{\mathrm{p}})$, the stress increment in the effective stress space yields (for a strain increment in the physical space):

$$\mathrm{d}\hat{\sigma}_{ij} = (1-D)C_{ijkl}(\mathrm{d}\varepsilon_{kl} - \mathrm{d}\varepsilon_{kl}^{\mathrm{p}}). \tag{9}$$

Since $\mathrm{d}\hat{\sigma}_{\mathrm{e}} = 3\hat{s}_{ij}\mathrm{d}\hat{\sigma}_{ij}/(2\hat{\sigma}_{\mathrm{e}})$ the expression for the physical plastic strain increment $\mathrm{d}\varepsilon_{ij}^{\mathrm{p}}$ can be written as:

$$\mathrm{d}\varepsilon_{ij}^{\mathrm{p}} = \chi h \hat{s}_{ij}\hat{s}_{kl}\mathrm{d}\hat{\sigma}_{kl}, \quad \text{where}$$
$$h = \frac{9}{4E\hat{\sigma}_{\mathrm{e}}^2}(E/E_{\mathrm{P}} - 1) \quad \text{and} \quad \chi = \begin{cases} 1 & \text{for } \hat{\sigma}_{\mathrm{e}} = H \text{ and } \mathrm{d}\hat{\sigma}_{\mathrm{e}} \geqslant 0 \\ 0 & \text{else} \end{cases} \tag{10}$$

A modified Ramberg–Osgood relation is assumed and the relation $E/E_{\mathrm{P}} = (\hat{\sigma}_{\mathrm{e}}/\sigma_0)^{n-1}$ where E is the Young's modulus for the virgin material, E_{P} the tangent modulus and $n \geqslant 1$ denote a hardening exponent. Following standard procedures commonly used in theories of plasticity (may be found in any textbook on the topic), the damage-elastic–plastic incremental stress–strain relation for plastic yielding in effective space can be written as:

$$\mathrm{d}\hat{\sigma}_{ij} = [(1-D)C_{ijkl} - \gamma L_{ij}L_{kl}]\mathrm{d}\varepsilon_{kl}, \text{ where}$$
$$L_{ij} = (1-D)C_{ijkl}\frac{3\hat{s}_{kl}}{2\hat{\sigma}_{\mathrm{e}}} \text{ and } \gamma = \begin{cases} \frac{4\hat{\sigma}_{\mathrm{e}}^2 h/9}{1+h\hat{s}_{ij}(1-D)C_{ijkl}\hat{s}_{kl}} & \text{for } \hat{\sigma}_{\mathrm{e}} = H \text{ and } \mathrm{d}\hat{\sigma}_{\mathrm{e}} \geqslant 0 \\ 0 & \text{else.} \end{cases} \tag{11}$$

Needless to say, for an undamaged material the expression within the brackets in (11) represents the well-known classic incremental elastic–plastic stiffness tensor.

During damage evolution the physical stress increment is obtained by differentiating (1), i.e.,

$$d\sigma_{ij} = (1 - D)d\hat{\sigma}_{ij} - dD\hat{\sigma}_{ij}, \tag{12}$$

where $d\hat{\sigma}_{ij}$ is determined by (11).

3. Verification for strains at mode I tensile fracture

In this section the theory described above is evaluated. The considered low-density paper has been designed to ensure bond–breakage as the dominating damage mechanism. The bonds have intentionally been kept weak relative the strength of the fiber and the degree of bonding low. The paper was manufactured at very low speed in a so-called trough air drying (TAD) process resulting in a sparse network having approximately isotropic mechanical properties. The material was made from bleached unbeaten softwood chemical pulp to a basis weight of 20 g/m^2. It has a length-averaged fiber length of 2.2 mm and width of 23.85 μm. In paper of this type there exist significant inherent variations (formation) in the structural properties, which is a result of the manufacturing procedure. Fig. 2 shows a photograph of the fiber network. Sparse regions in the material are seen as dark spots.

3.1. Experiment on a rectangular specimen containing a pre-fabricated slit

A tensile loaded rectangular body containing a pre-fabricated slit is examined. The analysis corresponds to a rectangular central cracked specimen during tensile mode I loading (opening mode). Such analysis enables evaluation of the non-local feature of the constitutive model because damage is localized to process zones developing at tips of the notches. The geometry of the notched specimen is visualized in Fig. 3. A quarter region is analyzed owing to the symmetry of the boundary conditions and loading.

Load–displacement response was measured in a MTS servo-hydraulic tensile test machine using specimens having width 395 mm ($2w$) and gauge length 230 mm ($2h$) at a deformation rate of 2.0 mm/min. The pre-fabricated crack was manually cut with a razor blade in the center of the specimen to a length 60 mm ($2a$). Since paper is strongly influenced by moisture, mechanical testing of paper must be carried out under humidity and temperature control in order to obtain reproducible results. The climate used was 23 °C and 50% RH (that is in accordance with ISO 187) and the samples were conditioned for at least 48 h in this environment prior to testing.

3.2. Full field strain measurement

An optical non-contact 3D displacement measuring system (Aramis HR) manufactured by GOM has been used to determine the strain field in the crack-tip region of a pre-fabricated crack in the fracture test

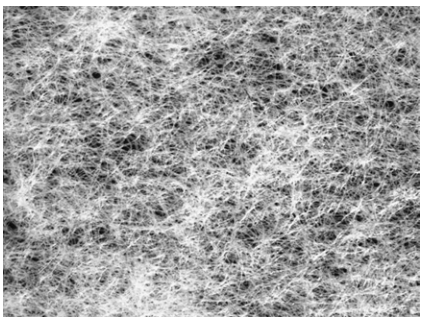

Fig. 2. Photograph of the considered fiber network. Sparse regions in the material are seen as dark spots.

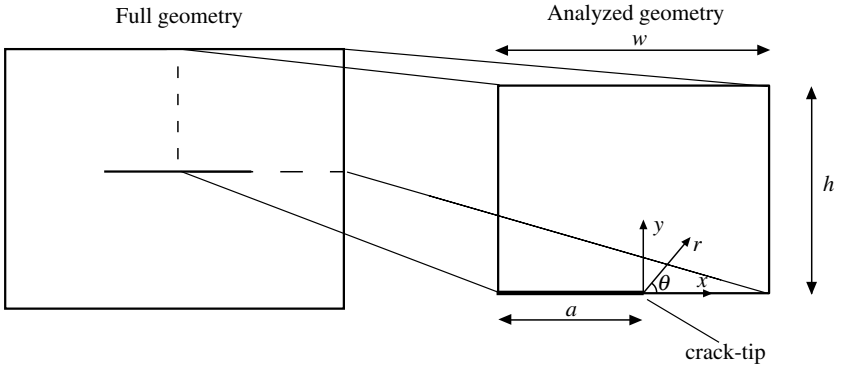

Fig. 3. Center cracked specimen.

described above. Fig. 4 shows the test set-up. The system monitors the surface of the specimen using a pair of CCD cameras (mounted on a stand) having a resolution of 1280×1024 pixels. A sequence of photographic images, for a number of pre-defined load levels, is recorded during the process of loading. The 3D coordinates of the deformed object surface are calculated by the system. For most materials a random or regular pattern must be applied to the surface of the specimen, which deforms along with the object. The equipment used works on both random and regular pattern. However, for the specific material considered in this investigation the specimens need no preparation because the inherent pattern that is due to random variations in the density and thickness is a sufficient reference pattern. However, to improve the contrast in the pattern, a light source was placed behind the specimen during loading. The deformation of a 30×30 mm domain ahead of the crack-tip was measured. The system divides the first image in a number of sub-images (15×15 pixels) called macro-image facets. Using an image correlation algorithm, these facets are tracked in each successive image with sub-pixel accuracy. Then, from the correlation procedure, a complete displacement field is obtained. By numerical spatial differentiation of the displacement field an approximation of the strain field is determined. The test set-up used in this study gives an accuracy of below 0.02%.

3.3. Numerical implementation and boundary conditions

Introduce a Cartesian (x,y) and a polar coordinate system ($r = [x^2 + y^2]^{1/2}$, $\theta = \tan^{-1}[y/x]$) with their origins coinciding with a crack-tip. The boundary conditions of the reduced geometry shown in Fig. 3 is given by:

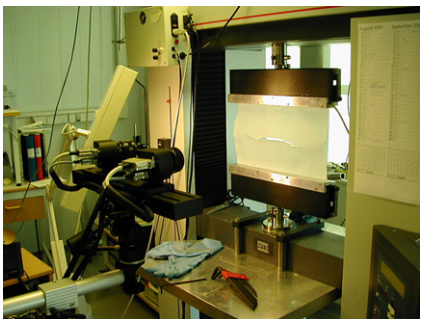

Fig. 4. Set-up of the optical non-contact 3D displacement measuring equipment.

$$\begin{aligned}
&\sigma_x = \tau_{xy} = 0 \quad \text{for } x = w - a \\
&u_y = \tau_{xy} = 0 \quad \text{for } 0 \leqslant x \leqslant w - a \text{ and } y = 0 \\
&\sigma_y = \tau_{xy} = 0 \quad \text{for } -a \leqslant x < 0 \text{ and } y = 0 \\
&u_x = \tau_{xy} = 0 \quad \text{for } x = -a \\
&u_x = 0 \text{ and } u_y = u_0 \quad \text{for } y = h
\end{aligned} \tag{13}$$

The displacements in the x- and y-directions are denoted u_x and u_y, respectively. σ_x and σ_y are the normal stresses and τ_{xy} is the shear stress. Additionally, the natural boundary condition of a vanishing gradient of $\overline{Y}$ on the boundaries is used.

The problem has been analyzed using the finite element method. The finite element procedure follows mainly the ones discussed in Peerlings et al. (1996) and Geers (1997) for an enhanced gradient model. Four-node isoparametric elements with two degrees of freedom, translation in the x- and y-directions, have been utilized. The entire mesh, representing a symmetric part of the body, consists of 15 138 elements. As a consequence of the damage processes that may occur around a dominant singularity, the material in the near-tip region eventually become non-linear and inhomogeneous and the stress-field looses its initial square-root singularity as $r \to 0$. For this reason, four-node elements are utilized rather than eight-node elements that are common in fracture mechanics models. This will be illustrated further in Section 4.

An iterative technique has been employed to solve the equilibrium equations at each load step. The result obtained after each iteration then corresponds to estimates of the incremental displacements from which the current stress and damage fields are computed. The numerical scheme was implemented in the Matlab (2002) code. All deformations are assumed to be small so that linear relations for equilibrium and kinematics are applicable and all derivatives and integrals are evaluated with respect to the initial topology of the considered body. A non-local formulation of the constitutive law guarantees that no spurious effects arise in the numerical solution. Fracture loads are numerically predicted when the overall damage of a material point in the near-tip region (process zone) reaches the critical value 1.

3.4. Calibration of the constitutive model

Acoustic emission (AE) has been used to detect the onset of the damage processes. Work carried out (among others: Salminen et al., 2003; or Yamauchi, 2004) has shown that the way paper fractures in tensile experiments can be followed by acoustic sensors and that the measured signals are closely related to the damage processes occurring within the paper's structure. The basic principle in AE is that during the fracturing of a fiber-to-fiber bond (which will occur in the order of μs), stresses in the neighborhood of the fracture site will be redistributed and cause a rapid release of elastic energy. This redistribution will in general be transmitted through the material as an elastic wave, which can be recorded on the surface of the material using an appropriate acoustic emission sensor. In this way each micro fracture is the source of one acoustic emission event. Eventually, the micro fracture density becomes so severe as the material collapse is measurable in tensile tests as a reduction of the stiffness. A computer was used to control the load frame and also to record data during the testing. The AE sensor, which is a piezoelectric 300 kHz resonance frequency sensor manufactured by AET, was positioned in the center point of each specimen. The sensor was held attached to the samples during the tests with a magnetic holder placed on the alternate side of the paper specimen. The AE signals were recorded by using a system manufactured by Vallen Systeme.

The principal directions of material symmetry of paper are defined as the machine direction (MD), which is the direction of manufacture, cross direction (CD), which is the transverse web direction and thickness direction (Z). The ratio between elastic modulus in MD and CD (anisotropy) was for the considered material 1.03 and between fracture stress 1.08. Also, the ratio between the yield stress in the two directions was ≈1.03. Hence, the paper material is approximately in-plane isotropic. For the calibration procedure, specimens having a width 80 mm and a length 10 mm were manufactured. The specimens were loaded in MD only, Fig. 5. The coefficient of variation was ≈4% for both the elastic modulus and yield stress and ≈6% for the fracture stress for a series of eight specimens. It is observed in Fig. 5 that onset of plastic yielding occurs

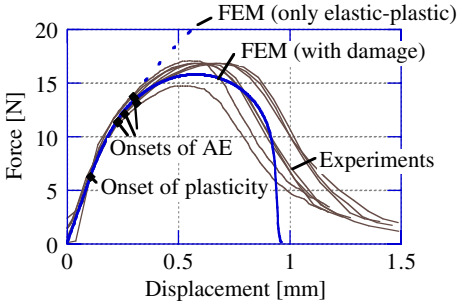

Fig. 5. Force–displacement curves measured in tensile experiments. Also shown is a computed result (FEM) when utilizing the damage theory described in Section 2, contrasted with a computed result obtained when using exclusively the classical elastic–plastic J_2-theory. Onsets of AE and plastic yielding are indicated in respectively experiment.

at a lower load than onset of the damage process (AE). With reference to Fig. 5, the mean force F_0 at which onset of AE occurred was determined to $F_0 = 12.55 \pm 1.1$ N. The relatively large interval of F_0 is due to significant inherent variations in the fiber network. Assuming that the stress field is approximately homogenous, then $Y_0 t = [F_0/W]^2(1-\nu^2)/Et$ where t and W is the thickness and width of the paper specimen. The Young's modulus per unit thickness $Et = 7.4$ kN/m was determined from the initial slopes of the force–displacement curves. The Poisson's ratio was set to $\nu = 0.29$ following Baum et al. (1981) and the onset of damage was determined to $Y_0/E = 0.41 \times 10^{-3}$. The damage parameter k was determined by fitting a force–displacement curve, calculated by the finite element model, to the experiments (Fig. 5). Similarly, the plasticity material parameters σ_0 and n were determined by fitting a calculated force–displacement curve, by the finite element model, to the experiments in the non-linear region located in-between the onsets of plastic yielding and of damage processes (AE). The determined values are: $\sigma_0/E = 1.1 \times 10^{-2}$, $n = 1.95$ and $kY_0 = 9.5 \times 10^{-2}$.

4. Results and discussion

Fig. 6 shows a typical force–displacement curve measured in a tensile test performed on a notched specimen. The final fracture initiates in the experiment in the neighborhood of peak-load. Also indicated in Fig. 6 are computed force–displacement curves when different values of the characteristic length l have been utilized, together with respective loads at which fracture initiates. At fracture load, the computed level of damage $D \to 1$ in the process zones whereupon onsets of macroscopic crack growth occurs.

According to Fig. 6 there seems to be a good agreement between the model and experiment for a characteristic length $l \approx 4.5$ mm, which is roughly twice the size of the length-averaged fiber length. This is in agreement with previous investigations by the authors on various paper materials (cf. Isaksson et al., 2004; or Hägglund and Isaksson, in press). Whether there is a relation between the two quantities should be

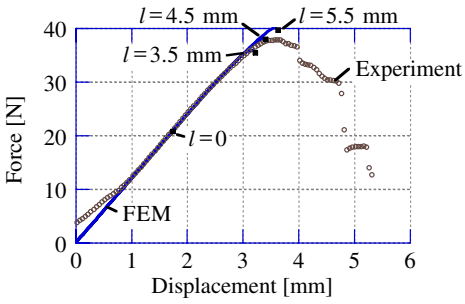

Fig. 6. A typical force–displacement curve measured in a fracture test on a notched specimen. Also shown are computed force–displacement relations and locations of onsets of final fractures when utilizing various characteristic lengths l (black squares).

investigated in a forthcoming study where the coupling between the fiber length and the intrinsic length parameter in the non-local model should be evaluated. The computed fracture load when using $l = 4.5$ mm is 38 N, which is the same as the fracture load obtained in experiment.

Fig. 7 shows the distribution of (physical) strains ε_y in the crack-tip region at various r and θ picked at loads corresponding to 87% (33 N) and 95% (36 N) of peak-load (see Fig. 6 for reference) for one single experiment. The latter load is the load immediately before onset of the final fracture obtained in experiment. Both calculated and experimentally determined strains are displayed along directions $\theta = 0$ and $\theta = \pi/4$. The strains are normalized with ε_y^∞, which is the asymptotic ε_y-strain far away from the crack-tip. For the sake of illustration, corresponding strains computed considering solely an elastic–plastic material (i.e., a pure J_2-flow theory) picked at the same loads are shown as well (i.e., for a situation with no damage processes present in the material). The maximum damage in the process zone in front of the crack-tip for the two considered loads is $D = 0.3$ and $D = 0.5$, respectively. As mentioned in Section 2, the non-linear relation $(1 - D)^2$ reflects the level of degradation of the elastic stiffness tensor.

In Fig. 7 the variation of thickness and density in the sheet is reflected in that the strain-field fluctuates and only agrees with the model in an average sense. The local variations in material properties are relatively high for the considered material. It should be said that no study of variation of strains between experiments has been made for the mode I loading case. However, for the considered material, the coefficient of variation in tensile testing of unnotched specimens is ≈4% for the elastic modulus and 6% for the peak load for a series of eight test specimens as discussed in Section 3.

Fig. 8 shows the strain ε_x along the crack plane when the load is 95% of peak-load. It is here observed that the difference between the continuum damage theory and the pure elastic–plastic theory is not as striking as for the ε_y-strain. This is not surprising as under mode I loading the dominant normal strain is ε_y, which is realized when comparing Figs. 7 and 8.

Fig. 9 shows a comparison between strains ε_y, normalized with $\varepsilon_0 = \varepsilon_y(r)$ when $l = 4.5$ mm, when using different characteristic lengths l and when using the pure elastic–plastic solution. When comparing Figs. 7 and 9, it is realized that the selected characteristic length $l = 4.5$ mm indeed seems to capture the strain ε_y well in the process zone. Also, it is illustrated that the magnitude of strains is highly influenced by the choice of l.

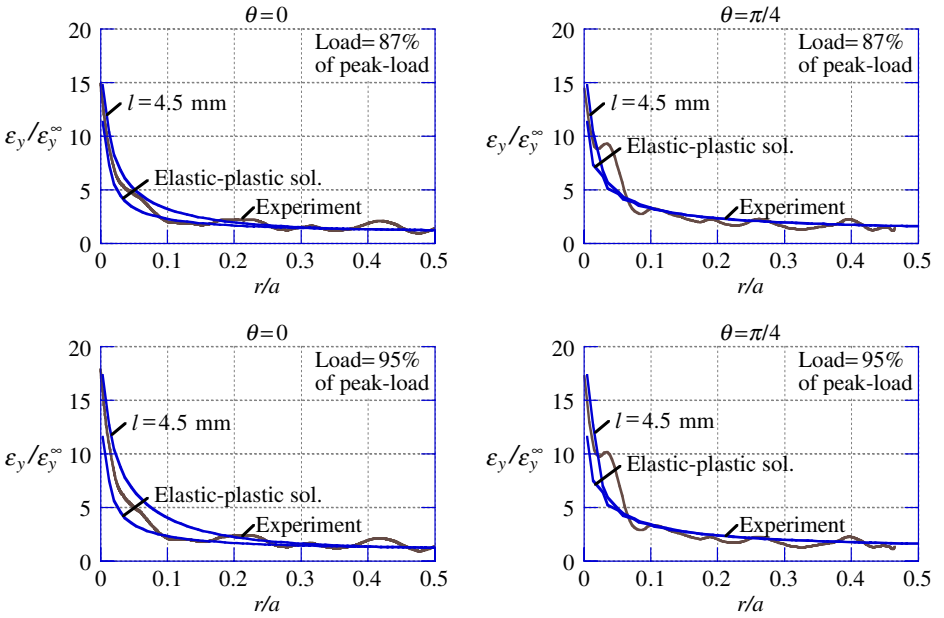

Fig. 7. Normalized strains $\varepsilon_y/\varepsilon_y^\infty$ for $r/a > 0$ along $\theta = 0$ and $\theta = \pi/4$ when the load is 87% and 95% of peak-load. Also shown are strains according to exclusively an elastic–plastic J_2-flow theory as well as experimentally measured strains at the corresponding loads.

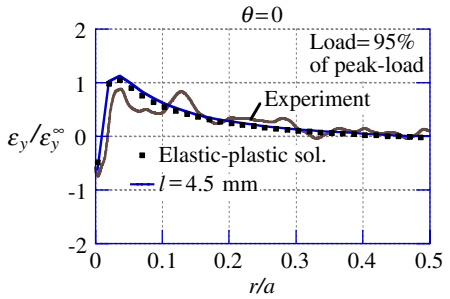

Fig. 8. Strain $\varepsilon_x/\varepsilon_x^{\infty}$ along the crack plane when the load is 95% of peak-load. Also shown is the strain according to the pure elastic–plastic J_2-flow theory as well as the experimentally measured strain at the corresponding load.

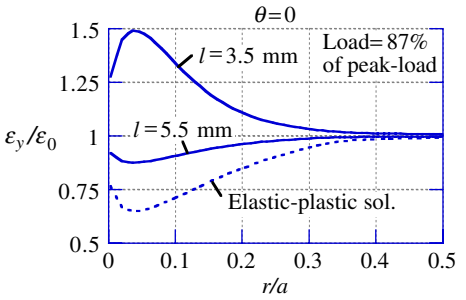

Fig. 9. Calculated strain ε_y in the vicinity of a crack-tip at the load corresponding to 87% of peak-load when utilizing different characteristic lengths l and for the pure elastic–plastic solution. The strains are normalized with $\varepsilon_0 = \varepsilon_y(r)$ when $l = 4.5$ mm.

The results shown in Figs. 7–9 implies that the investigated paper material may tolerate significantly higher strains than what is indicated by the classic elastic–plastic J_2-flow theory when computing strains at the load corresponding to peak-load. Immediately before the final fracture the experimental measured normal strain ε_y is around 60% higher than the computed strain obtained when using exclusively the elastic–plastic J_2 theory. The normal strain computed utilizing a non-local damage theory is of the same order of magnitude as the experimentally measured strain. Hence, it seems essential to include a non-local damage theory to describe strains in the near-tip region quantitatively correct for this class of materials. This is an important result and confirms earlier published results. Recently, Wathén et al. (2005) reported, in a experimental study that considers the straining mechanism in paper during a fracture process, that their results indicates that paper materials seems to stand much higher local strains than what is suggested by classical theories. To be able to fully understand the processes behind the material degradation in a process zone in paper materials, it is of significant interest to dwell deeper into the mechanisms controlling the observed non-local phenomenon. This is a subject of a forthcoming study.

It is also of interest to evaluate the stresses acting in the crack-tip region. Fig. 10 shows computed normal stresses σ_y along the crack plane in front of the tip immediately before onset of final fracture. Hence the shown stresses are picked for the same situation as the strains shown in Fig. 7(c). The stresses are normalized with σ_y^{∞}, which is the asymptotic normal stress σ_y far away from the crack-tip. In Fig. 10 both the physical and effective stresses are shown. Again, it is noted that the effective stress $\hat{\sigma}_{ij}$ is referred to a surface in the material that really transmits the internal forces.

As can be seen, the computed effective stress $\hat{\sigma}_y$ is around 30% higher in the near-tip region according to the non-local damage theory as compared to the pure elastic–plastic J_2 theory for the corresponding load. Fig. 10

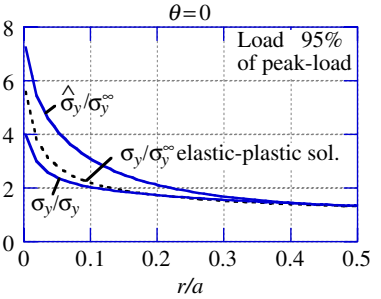

Fig. 10. Stresses σ_y and $\hat{\sigma}_y$, normalized with σ_y^∞, along the crack plane immediately before onset of final fracture.

further illustrates the importance of including a damage theory when studying strains and stresses around singularities for this class of materials.

4.1. A note on the singularity of stress and strain

Hutchinson (1968) and Rice and Rosengren (1968) showed that in order to remain path independence of the well-known J-integral (Rice, 1968) in a non-linear elastic–plastic material, the stress and strain must vary near the crack-tip according to (cf. Anderson, 1991):

$$\rho\sigma_{ij}\varepsilon_{ij} = r^{\alpha}, \tag{14}$$

where ρ is a proportionality constant and the exponent $\alpha = -1$. To illustrate that this relation in general not is valid for a non-local continuum damage model, the logarithmic form of (14) is studied. Fig. 11 shows the computed values of $\log[\sigma_y\varepsilon_y/\varepsilon_y^\infty]$ versus $\log[r/a]$ at the moment of fracture, i.e., at the load when $\max\{D\} \to 1$. The exponent α is determined by fitting a polynomial $\log[\sigma_y\varepsilon_y/\varepsilon_y^\infty] = \alpha\log[r/a] + \text{const}$ that fits the computed data in a least-square sense. The result according to the non-local damage theory ($l = 4.5$ mm) is shown as well as the result according to the pure elastic–plastic J_2-flow theory for the corresponding load. When using exclusively an elastic–plastic material description $\alpha = -1.00$ and confirms earlier results. In this case the well-known HRR-solutions (Hutchinson, 1968; Rice and Rosengren, 1968) are achieved, which describe the nature of the dominant singularity in the vicinity of the crack-tip. However, when using a non-local continuum damage-elastic–plastic material formulation, $\alpha \neq -1$ and thereby demonstrates that path independence of the J-integral does not prevail for this class of material models. This result is not surprising, as energy has dissipated from the system when damage has evolved in the material. Only for the special situation of a homogenous damage field in the crack-tip region may the stress and strain fields be described by the HRR-solutions. A modification of the HRR-solutions to include a damage field is not straightforward as the damage distribution is controlled by the length l and varies with r, as illustrated in Fig. 11(b).

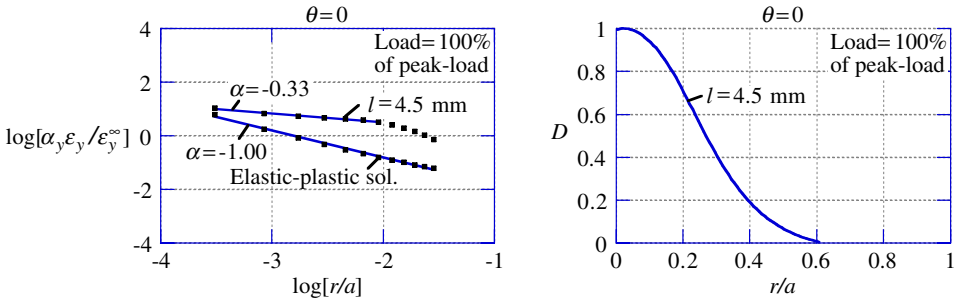

Fig. 11. (a) Log–log diagrams of (14) when use is made of a non-local damage theory at fracture load and a classic pure elastic–plastic theory at the corresponding load. (b) Damage distribution in front of the tip along the crack plane at fracture load.

5. Conclusions

Strains, computed by the finite element method, are in this investigation compared to an experimentally determined strain field. The considered low-density paper has been designed to ensure bond–breakage as the dominating damage mechanism and the paper material is approximately in-plane isotropic. An optical non-contact displacement measuring system has been used in fracture tests to determine the strain field in the crack-tip region of a pre-fabricated crack. Additionally, acoustic emission monitored tensile tests have been conducted to determine onset and evolution of damage processes in a homogenous stress field and thereby enabling calibration of the required constitutive parameters. The obtained results suggest that the investigated paper material can tolerate significantly higher strains than what is predicted by the classic elastic–plastic J_2-flow theory. Immediately before onset of the final fracture, the experimental measured normal strain is around 60% higher than the computed strain when using exclusively an elastic–plastic theory for the same load while the normal strain computed utilizing a non-local damage theory is of the same order of magnitude as the experimentally measured strain. Hence, it seems essential to include a non-local continuum theory to describe strains in the near-tip region quantitatively correct for paper materials. It is demonstrated that path independence of the well-known J-integral does not prevail for this class of material models. Only for the special situation of a homogenous damage field in the crack-tip region may the stress and strain fields be described by the HRR-solutions.

Acknowledgements

Rickard Styverts at SCA Research is acknowledged for assistance with the Aramis system. The Swedish Foundation Program for Knowledge and Competence Development (KK Foundation) and the Bo Rydin Foundation are acknowledged for financing this work.

References

Abu Al-Rub, R.K., Voyiadjis, G.Z., 2003. On the coupling of anisotropic damage and plasticity models for ductile materials. Int. J. Solids Struct. 40, 2611–2643.

Anderson, T.L., 1991. Fracture Mechanics: Fundamentals and Applications. CRC Press, Boca Raton, USA.

Baum, G.A., Brennan, D.C., Habeger, C.C., 1981. Orthotropic elastic constants of paper. Tappi 64, 97–101.

Chow, C.L., Lu, T.J., 1992. An analytical and experimental study of mixed-mode ductile fracture under nonproportional loading. Int. J. Damage Mech. 1, 191–236.

de Borst, R., Pamin, J., Geers, M.G.D., 1999. On coupled gradient-dependent plasticity and damage theories with a view to localization analysis. Eur. J. Mech. A/Solids 18, 939–962.

Eringen, A.C., Edelen, D.G.B., 1972. On nonlocal elasticity. Int. J. Eng. Sci. 10, 233–248.

Geers, M.G.D., 1997. Experimental analysis and computational modelling of damage and fracture. Ph.D. thesis. Eindhoven University of Technology, The Netherlands.

Hägglund, R., Isaksson, P., in press. Analysis of localized failure in low-basis-weight paper. Int. J. Solids Struct., doi:10.1016/j.ijsolstr.2005.08.016.

Hansen, N.R., Schreyer, H.L., 1994. A thermodynamically consistent framework for theories of elastoplasticity coupled with damage. Int. J. Solids Struct. 31, 359–389.

Hutchinson, J.W., 1968. Singular behavior at the end of a tensile crack in a hardening material. J. Mech. Phys. Solids 16, 13–31.

Hutchinson, J.W., 1987. crack-tip shielding by micro-cracking in brittle solids. Acta Metall. 35, 1605–1619.

Isaksson, P., Hägglund, R., 2005. A mechanical model of damage and delamination in corrugated board during folding. Eng. Frac. Mech. 72, 2299–2315.

Isaksson, P., Hägglund, R., Gradin, P., 2004. Continuum damage mechanics applied to paper. Int. J. Solids Struct. 41, 4731–4755.

Isaksson, P., Gradin, P.A., Kulachenko, A., 2006. The onset and progression of damage in isotropic paper sheets. Int. J. Solids Struct. 43, 713–726.

Jirásek, M., 1998. Nonlocal models for damage and fracture: Comparison of approaches. Int. J. Solids Struct. 35, 4133–4145.

Kröner, E., 1967. Elasticity theory of materials with long range cohesive forces. Int. J. Solids Struct. 3, 731–742.

Lasry, D., Belytschko, T., 1988. Localization limiters in transient problems. Int. J. Solids Struct. 24, 581–597.

Matlab, 2002. Version 6.5. The MathWorks Inc., Natick, MA, USA.

Mühlhaus, H.B., Aifantis, E.C., 1991. A variational principle for gradient plasticity. Int. J. Solids Struct. 28, 845–857.

Niskanen, K.J., 1993. Strength and fracture of paper. KCL Paper Science Centre, Espoo, Finland.

Ortiz, M., 1987. A continuum theory of crack shielding in ceramics. J. Appl. Mech. 54, 54–58.

Peerlings, R.H.J., de Borst, R., Brekelmans, W.A.M., de Vree, J.H.P., 1996. Gradient enhanced damage for quasi-brittle materials. Int. J. Num. Meth. Eng. 39, 3391–3403.

Pijaudier-Cabot, G., Bazant, Z.P., 1987. Nonlocal damage theory. J. Eng. Mech. 113, 1512–1533.

Ravichandran, G., Liu, C.T., 1998. crack-tip shielding in elastic particulate composites undergoing damage. Eng. Frac. Mech. 59, 713–723.

Rice, J.R., 1968. A path independent integral and approximative analysis of strain concentration by notches and cracks. J. Appl. Mech. 35, 379–386.

Rice, J.R., Rosengren, G.F., 1968. Plane strain deformation near a crack-tip in a power law hardening material. J. Mech. Phys. Solids 16, 1–12.

Salminen, L.I., Tolvanen, A.I., Alava, M.J., 2003. Acoustic emission from paper fracture. Phys. Rev. Lett. 89, 185503, 1–4.

Swineheart, D., Broek, D., 1995. Tenacity and fracture toughness of paper and board. J. Pulp Paper Sci. 21, J389–J397.

Wathén, R., Batchelor, W., Westerlind, B., Niskanen, K., 2005. Analysis of strains in the fracture process zone. Nordic Pulp Paper Res. J. 20, 392–397.

Westerlind, B.S., Carlsson, L.A., Andersson, Y.M., 1991. Fracture toughness of linerboard evaluated by the *J*-integral. J. Mat. Sci. 26, 2630–2636.

Yamauchi, T., 2004. Effect of notches on micro failures during tensile straining of paper. Japan Tappi J. 58, 105–112.